

Resistance Microwelding of Ti-55.8 wt pct Ni Nitinol Wires and the Effects of Pseudoelasticity

BILLY TAM, ANDREW PEQUEGNAT, MOHAMMAD IBRAHEEM KHAN,
and YUNHONG ZHOU

Nitinol has revolutionized many traditional engineering designs with its unique properties that include pseudoelasticity and the shape-memory effect (SME). However, the general lack of understanding on welding Nitinol limits its full potential in practical applications. The current study examined the microstructure and mechanical properties of resistance microwelded (RMW) Ni-rich Nitinol wires at different applied currents. The results revealed a solid-state bonding mechanism that consisted of six main stages, including (1) cold collapse, (2) dynamic recrystallization, (3) interfacial melting, (4) squeeze out, (5) excessive flash, and (6) surface melting. The joint strength and fracture mechanism were linked closely to the metallurgical properties of the welds. Through differential scanning calorimetry (DSC) testing, it was found that the weld metal underwent phase transformation at lower temperatures compared with the base material. Also, the pseudoelastic property of Nitinol was found to have a large effect on the contact resistance during the onset of welding current. Compression tests with varying temperatures confirmed distinct differences in displacement (*i.e.*, cold collapse) under the welding load of 5 kg-f caused by changes in the thermodynamic stability of the austenite phase. Both the dynamic resistance and displacement measurements were found to be significantly different during the RMW of Nitinol crossed wires compared with welding 316 low-vacuum melted (LVM) stainless steel (SS) crossed wires.

DOI: 10.1007/s11661-012-1115-7

© The Minerals, Metals & Materials Society and ASM International 2012

I. INTRODUCTION

IN recent years, the interest in incorporating Nitinol components in dental and medical devices has increased because of the unique properties of pseudoelasticity, shape-memory effect (SME), and biocompatibility. Currently, Nitinol alloys are used in the fabrication of vascular stents, guidewires, and orthodontic arch wires.^[1] With the trend of miniaturization, other processing methods such as microwelding, are required to help meet this expectation.^[2] One method is to implement resistance microwelding (RMW) of crossed wires, which is a commonly used process for the electrical interconnection and component integration for devices such as pacemakers.^[2,3]

Resistance microwelding of crossed wires has been examined previously in the literature.^[3–6] The bonding mechanism is influenced strongly by process parameters (*i.e.*, welding current, electrode force, *etc.*), material properties (*i.e.*, resistivity, hardness, *etc.*), and surface condition (*i.e.*, oxide, roughness, *etc.*). For example, Fukumoto *et al.*^[3–5] found solid-state bonding to be the primary joining mechanism in Ni, NiTi, and 304

stainless steel (SS). In contrast, for medical grade 316 low-vacuum melted (LVM) SS, the optimized bonding mechanism was fusion welding.^[6] A few reported studies on resistance welding Nitinol showed solid-state bonding^[4,7]; however, detailed studies on the joining mechanism for Nitinol alloys and the effects of the process on material properties still remain scarce.^[8–10]

The functional properties of Nitinol are sensitive to thermomechanical processing. The modifications to base metal transformation behaviors^[11–13] and previous strengthening heat treatments^[14,15] have been shown to occur during the application of heat or mechanical deformation. For example, Kurita *et al.*^[12] showed that cold working widened the temperature range over which transformation occurred, whereas Frick *et al.*^[13] detailed the aging effects on hot-rolled and cold-rolled Nitinol. Similarly, various studies have used direct electric resistance heat treatment successfully to modify the hardness and stress-strain responses.^[14,15] Also, a laser microwelding study by Tam *et al.*^[8] using the same materials and crossed-wire joint configuration used in this work identified an increase and a decrease in the transformation temperatures of the fusion zone and heat-affected zone (HAZ), respectively. All the aforementioned publications emphasized that the functional properties of Nitinol are sensitive to thermal and mechanical treatments, which are similar to those experienced during RMW.

The objectives of this study were to (1) investigate the bonding mechanism using metallurgical examinations,

BILLY TAM, MASci, ANDREW PEQUEGNAT, PhD Student, and MOHAMMAD IBRAHEEM KHAN, Postdoctorate, and YUNHONG ZHOU, Professor, are with the Centre for Advanced Materials Joining, Department of Mechanical Engineering, University of Waterloo, Waterloo, ON N2L 3G1, Canada. Contact e-mail: apeqegn@uwaterloo.ca

Manuscript submitted May 2, 2011.

Article published online March 17, 2012

(2) detail the weld formation and its influence on mechanical performance, (3) characterize the phase-transformation behavior post-RMW, and (4) identify the challenges caused by pseudoelasticity and the SME of Nitinol during crossed-wire RMW.

II. EXPERIMENTAL PROCEDURES

A. Materials

Commercially available pseudoelastic NiTi wires with a 0.41-mm diameter were used in this study. The materials had a Ni content of 55.8 wt pct with balanced Ti (*i.e.*, Ni-rich alloy). The complete chemical composition as reported by the manufacturer is detailed in Table I. Previously, thermomechanical processing had been performed on the wires by the manufacturer to optimize pseudoelasticity at room temperature. Surface treatment using diluted solution of hydrofluoric acid and nitric acid (*i.e.*, 15 pct HF + 40 pct HNO₃ + Bal. H₂O) for 20 seconds was performed prior to welding to remove the thick, dark oxide layer resulting from previous processing.

The phase-transformation temperatures of the base material and welded samples were measured by differential scanning calorimetry (DSC) using a Thermal Analysis Q2000 system (TA Instruments, New Castle, DE) equipped with refrigerated cooling system. For the weld samples, the unaffected wire material around the weld was clipped off; however, some base material still remained. A modified version of the ASTM F2004-05 standard test method for transformation temperature of Nickel-Titanium alloys by thermal analysis was used, in which the testing temperatures ranged between 198 K and 373 K (−75 °C and 100 °C), controlled at a rate of 5 K per minute. The start and finish transformation temperatures, martensite start (M_s) and austenite finish (A_f), were determined as the intersections of tangents to the slope of maximum inclination of the corresponding peaks with the base line.

B. Resistance Microwelding Equipment and Parameters

The RMW equipment consisted of a MacGregor DC4000P (MacGregor Welding Systems, Suffolk, U.K.) direct current power supply and a Miyachi 300 series (Miyachi Unitek, Monrovia, CA) fast response weld head coupled to a $\pm 0.2 \mu\text{m}$ sensitivity Heidenhain displacement sensor. Cylindrical flat-ended class 2 Cu-Cr electrodes with a diameter of 3.2 mm were used. The wires were welded at right angles to each other using variable currents from 120 A to 295 A. The welding time was 10 ms with an upslope and downslope time of 2 ms; a welding force of 5 kg-f was applied during the

entire welding sequence. Short upslope and downslope times were chosen to enable fast heating and cooling.

Dynamic electrical signals (*i.e.*, current, interfacial resistances, and voltage) and displacement of the top electrode were monitored using a National Instruments data acquisition (DAQ) system (National Instruments Corporation, Austin, TX). Interfacial resistances at both electrode-to-wire interfaces and faying interface shown as R1, R3, and R2, respectively, in Figure 1(a) were analyzed. The displacement measurements were converted to a percentage of the embedment of the top wire into the bottom wire, which is referred to as set down in crossed-wire welding.

C. Mechanical Test and Microstructural Analysis

The joint performance of the crossed wires was expressed as joint breaking force (JBF). Microtensile and compression testing were conducted on an Instron 5548 microtensile tester (Instron Corporation, Norwood, MA) equipped with a temperature chamber. Crosshead speeds of 0.4 mm/min and 0.04 mm/min were used for the tensile and compression tests, respectively. Joint breaking force was measured using a tensile-shear test direction as illustrated in Figure 1(b). A minimum of five samples were tested at each welding condition. The tensile tests were designed to provide essential information for the practical application of crossed-wire NiTi welds. The purpose of the compression tests was to investigate the effects of the pseudoelastic properties of the base material on the RMW process. Weld cross-sections and fracture surfaces were examined by optical microscopy and scanning electron microscopy (SEM). Micro Vickers hardness was measured using a Shimadzu micro hardness tester (Shimadzu Corporation, Kyoto, Japan). A series of microhardness indents was made with 40 μm in between each indent on the longitudinal centerline of the weld cross sections using a 50-g-f load and 20 seconds dwell time. The metallographic samples were mounted in epoxy and then ground and polished before being etched with 14 mL HNO₃, 3 mL HF and 83 mL H₂O solution for 25 to 30 seconds.

Table I. Chemical Composition of 55.8 wt pct Ni-Ti in wt pct

Ni	Ti	C	O	Co	Fe	Cr	Cu	H	No
55.8	44.2	<0.050				<0.010		<0.005	<0.025

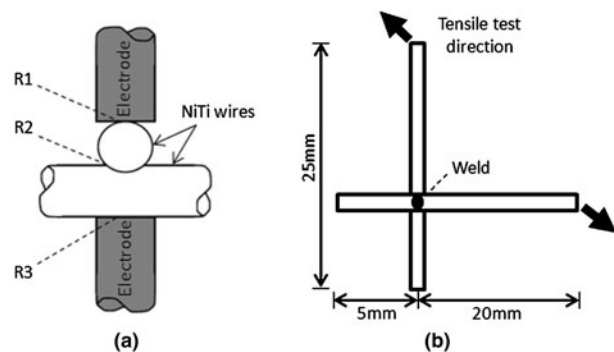


Fig. 1—Schematic illustrations of (a) welding setup and (b) tensile test direction (not to scale).

III. RESULTS AND DISCUSSION

A. Effects of Surface Oxides

The advantages of removing the surface oxide from Nitinol before resistance welding were realized in the dynamic resistance measurements. The dynamic resistance profiles of the welds made with acid-treated and untreated wires are shown in Figure 2. Dynamic resistance is characterized by an initial peak resistance followed by a sharp decrease occurring within the first few milliseconds.^[16–18] Subsequently, the resistance gradually decreases until the weld is completed. The acid-treated wires exhibited a decrease in peak resistances at all interfaces (R1, R2, and R3). The contact resistance between the electrodes and the wires and at the faying interface was decreased by removing the thick surface oxide and contaminants before welding. In general, the heat generation in RMW can be described using the following equation:

$$Q = I^2 R t \quad [1]$$

where I is the welding current and t is the welding time. The total resistance R is the sum of the contact resistances and the bulk resistances, which has a direct effect on the heat generation. Therefore, the decrease in the contact resistance in the acid-treated samples allowed for the use of higher currents before severe expulsion or sticking between the electrode and the wire occurred as a result of excessive heating at the faying interface or electrode wire interface, respectively. Also, the larger R2 relative to the R1 and R3 observed during RMW of the acid-treated sample enabled the resistive heating to concentrate at the faying interface promoting metallurgical bonding. Cleaning was also expected to result from acid treatments preventing the contaminants from being embedded in the microstructure during welding, which will subsequently improve joint quality and strength.

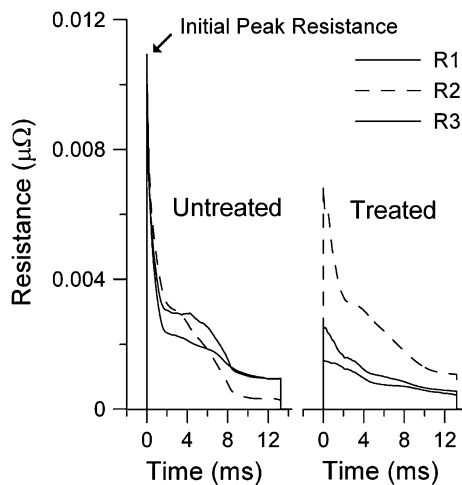


Fig. 2—Effects of acid treatment on interfacial resistances R1, R2, and R3.

B. Microstructure of Cross-Wire Joints

The cross-sectional profiles of the welds made with welding currents between 145 A and 295 A are shown in Figure 3. The heat generated near the interface during the initial application of current resulted in the recrystallization of the original fine-grained structure of the base metal in the HAZ, as shown in Figure 3(a). The bond interface was clearly visible at the welding currents of 145 A but was not present prior to etching. This suggests insufficient bonding likely because of the entrapment of surface defects and contaminants (Figure 3(b)).^[2] Both the base metal and the weld metal showed several finely dispersed precipitates in the microstructure, which are likely TiC compounds that formed during the production of the Nitinol ingot.^[19]

Increasing the welding current to 195 A resulted in widening of the HAZ (Figure 3(c)). The weld microstructure exhibited grain growth at the faying interface as suggested by the partial disappearance of the bond interface (Figure 3(d)). Squeezed out metal and surface contaminants, which are commonly referred to as flash material, was observed around the joint periphery, which was facilitated by the combination of initial high resistance heating at the faying interface and electrode force, which pushes the molten material toward the joint periphery.^[2] This partially molten flash material is shown in Figure 4. The weld microstructure at currents surpassing 245 A experienced subsequent widening of the HAZ and complete elimination of the bond interface, whereas an increased amount of flash material was expelled from the joint interface (Figures 3(e) and (f)). Complete (*i.e.*, 100 pct) set down was attained with welding currents of 295 A with columnar grains forming at the top and bottom surfaces of the joint caused by surface melting adjacent to the electrodes (Figures 3(g) and (h)). Finally, severe expulsion occurred when more than 295 A of current was applied, resulting in no joint formation.

The hardness measurements along the longitudinal centerline of the weld cross sections prepared at select currents are shown in Figure 5. The base metal hardness was approximately 400 Hv, which resulted from the fine-grained structure produced during the cold-drawing wire fabrication process. The hardness values decreased 30 to 35 pct, and the welds made with the highest currents showed the largest decrease. Softening in the welded region was more pronounced near the bond interface where the highest electrical resistance was measured (Figure 2). This decrease in hardness was caused by the recrystallization and growth of the cold-worked and heat-treated structure of the base metal. Similar softening effects were observed in the HAZ following LMW of fine crossed-wire NiTi.^[8]

The primary bonding mechanism resulting from RMW of the crossed Nitinol wires was found to be solid-state joining, which is similar to previous studies on Ni, NiTi, and 304 SS crossed wires.^[3–5] The joint morphology with the increasing weld current can be described in six stages. The initial cold collapse stage describes the mechanical deformation imposed by the electrode force from which a larger contact area was

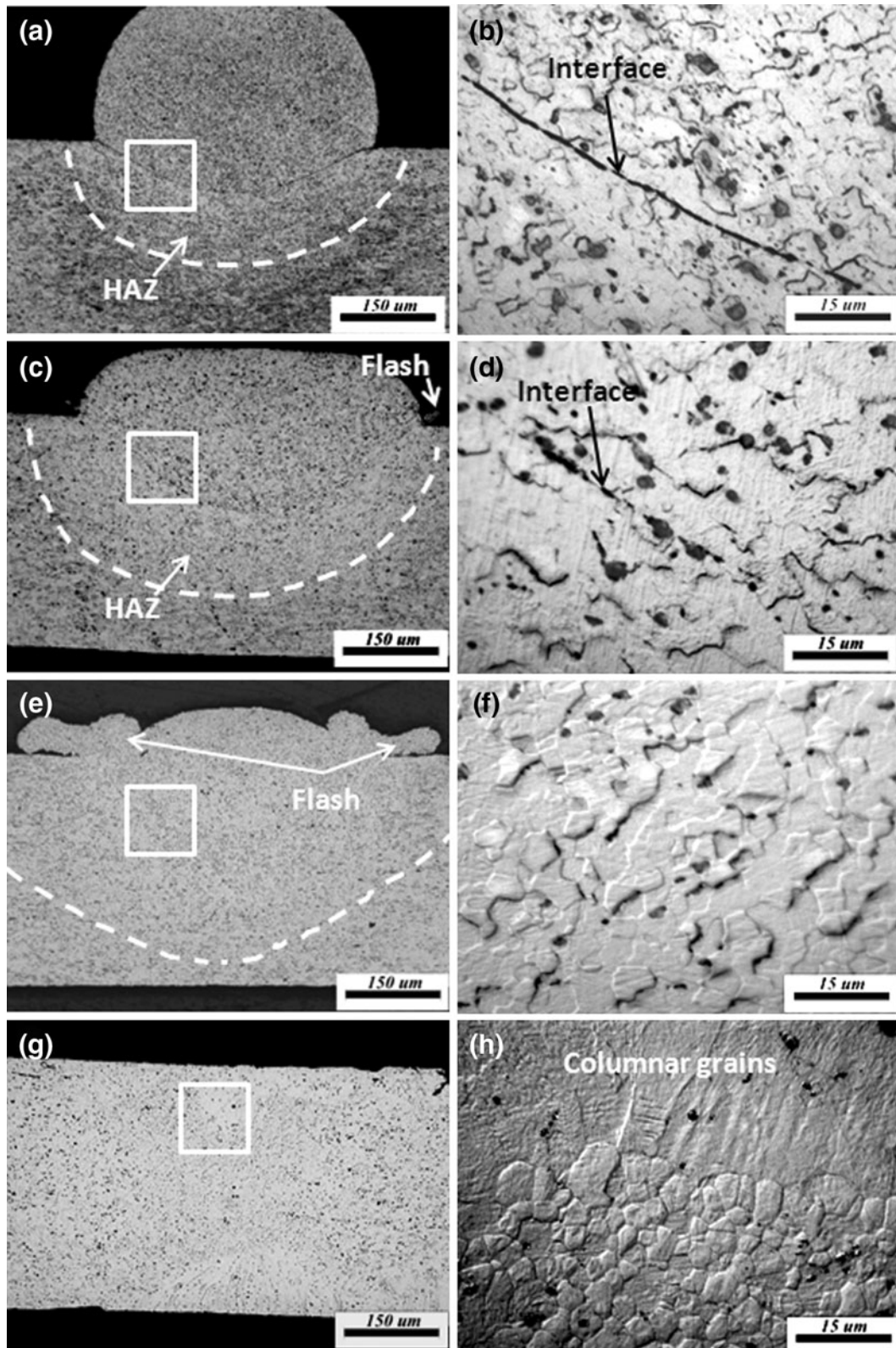


Fig. 3—Cross sections of joints welded with different currents; 145 A (*a* and *b*), 195 A (*c* and *d*), 245 A (*e* and *f*), and 295 A (*g* and *h*). HAZ located between bond interface and dashed lines.

formed. Subsequent application of welding current increased the temperature at the interface, resulting in dynamic recrystallization (*i.e.*, stage 2) of the fine-

grained base metal microstructure and softening in the HAZ. As the peak temperatures surpassed the solidus temperature at the interface, the interfacial melting stage

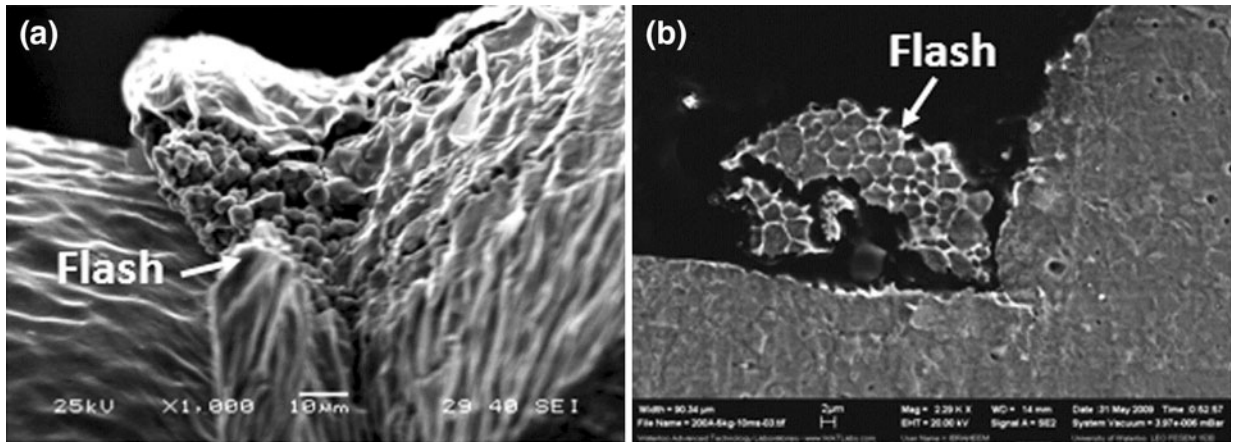


Fig. 4—Surface (a) and cross-sectional (b) scanning electron micrographs of flash material around the periphery of weld made using 195 A.

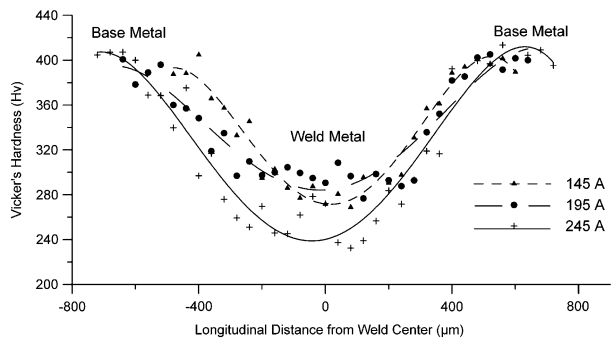


Fig. 5—Hardness along cross sections of welds made using various welding currents.

(i.e., stage 3) occurred, followed by a squeeze out stage (i.e., stage 4) where the electrode force pushed the partially molten metal toward the weld joint perimeter. This squeeze out stage is necessary for quality solid-state bonding as the contaminants are removed from the faying interface, improving the surface conditions for crystallographic matching and interdiffusion of atoms across the interface.^[2,5] A large amount of expulsion was detected with again increasing welding currents, leading to the excessive flash stage (i.e., stage 5) where the undesired weld defects were introduced. Subsequent increasing of the current-induced melting of the wire surfaces next to the electrodes in the surface melting stage (i.e., stage 6) and sticking of weld metal to the electrodes occurred, which affected the weld quality and electrode life significantly.^[20]

C. Mechanical Properties and Joint Breaking Force

The effects of the welding current on the set down and JBF are shown in Figure 6. Set down increased gradually with current and complete set down was attained at 295 A. A minimum welding current of 115 A was required to initiate bonding with JBFs increasing slightly up to 145 A. The joint strength improved sharply near 165 A followed by a more gradual increase up to 195 A, where the maximum JBF of 18 N was attained at 70 pct set down. A subsequent increase in the

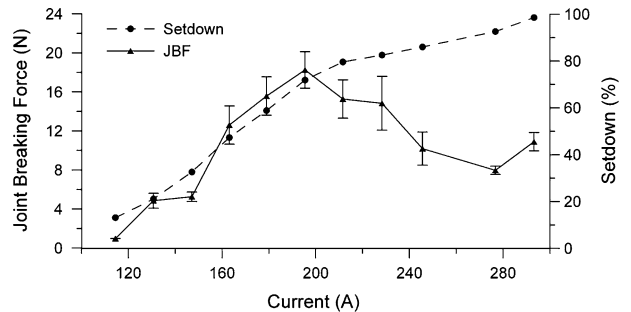


Fig. 6—Effects of welding current on JBF and set down.

current resulted in overwelding and degradation of joint strength because of the introduction of weld defects. Fukumoto *et al.*^[4] achieved a 58.8 N JBF with 0.34 mm diameter NiTi cross-wire RMW welds. However, the tensile testing method used was different, which made comparisons of JBF difficult.

The SEM micrographs of the fractured samples welded between 145 A and 245 A are presented in Figure 7. These images show that the joints failed in the welded region for all currents tested. The joint strength and fracture mechanism of RMW crossed-wire NiTi joints were influenced strongly by the weld morphology. Between 115 A and 145 A, at which low JBFs were attained, fracture occurred through the bond interface as shown in Figure 7(a). The relatively smooth fracture surface indicated a sudden brittle fracture mode at the dispersed local bonded sites (Figure 7(b)). By increasing the welding currents to 195 A and 245 A, the joint strength gradually increased because of increased set down (i.e., bond area) coupled with improved solid-state bonding resulting from the production of flash material. This increased joint strength was reflected by the dimpled ductile fracture morphology shown in Figure 7(d). However, in the 195 A fracture surface, the regions of the bond interface were still visible (Figure 7(e)). Discontinuities along the bond interface (Figure 3(d)) acted as stress raisers, resulting in fracture initiation at the interface, which then propagated through the softened HAZ. At higher currents, the HAZ became the preferred region for fracture as the bond strength

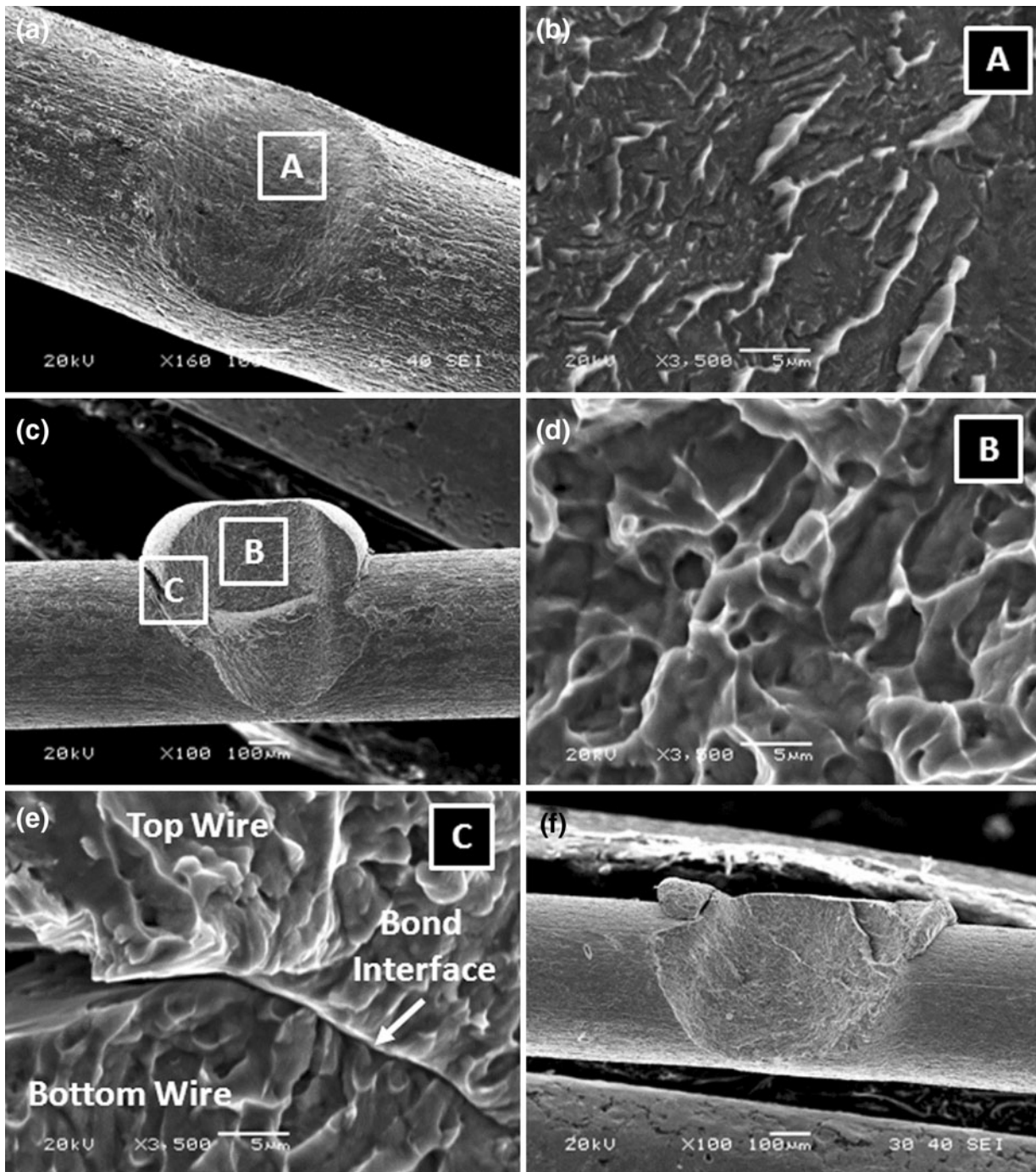


Fig. 7—Fracture surfaces of joint welded with different currents: 145 A (*a* and *b*), 195 A (*c* through *e*), and 245 A (*f*).

continued to improve while the HAZ was softened/weakened because of recrystallization (Figure 7(f)). Additionally, a sizeable separation at the joint edges was formed because the increased flash material created a notch effect. Figure 8 shows an SEM micrograph of a failed joint halted at the onset of failure during a tensile test with the fracture path indicated by an arrow. The stress concentrated at the notch tip during loading allowed cracks to penetrate easily into the HAZ and, therefore, reduced joint strength substantially.

The transition of fracture modes from interfacial at low currents (*i.e.*, 115 A to 145 A) to in the HAZ at high currents (*i.e.*, 210 A to 295 A) is shown schematically in Figure 9. Mixed mode failure occurred when using intermediate currents (*i.e.*, 165 A to 195 A), which is referred to as partial interfacial. Increasing the welding current creates a competition between two counterbalancing behaviors, increased interfacial bond strength, and wire softening, which improve and degrade the joint strength, respectively. The sum of their effects deter-

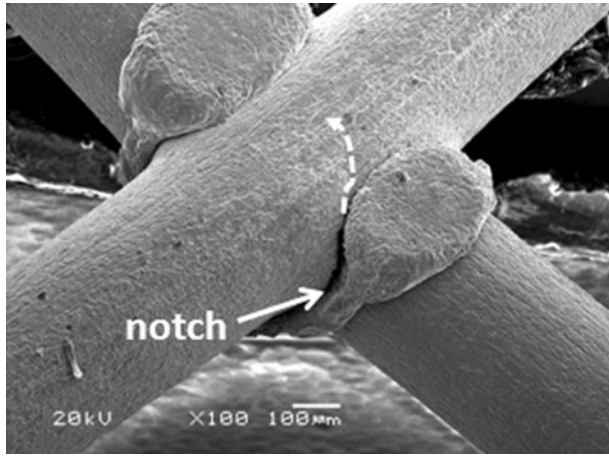


Fig. 8—Partial failure of weld made using 245 A welding current.

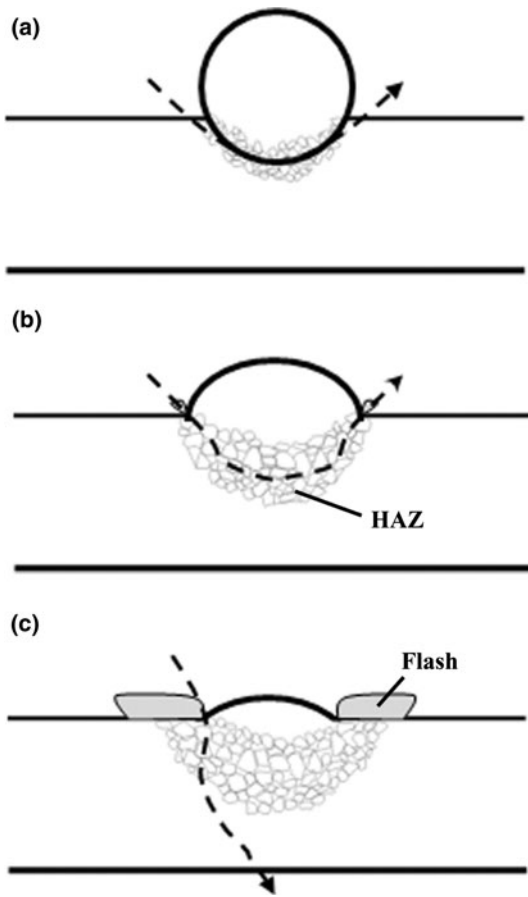


Fig. 9—Schematic of failure modes with increasing weld current: interfacial (a), partial interfacial (b), and HAZ (c).

mines the actual joint strength. At low currents, insufficient bonding led to interfacial failure, whereas at high currents, the joints failed through the softer HAZ. Maximum JBFs were obtained at intermediate welding currents when the bond strength and wire softening were better balanced.

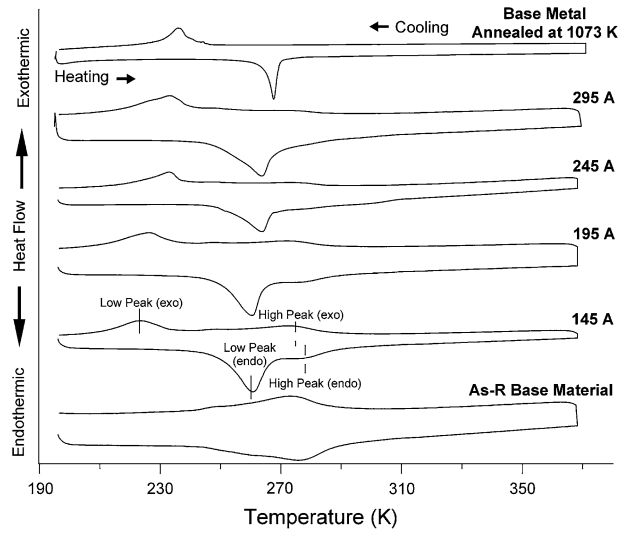


Fig. 10—DSC heating and cooling curves for the annealed wire, as-received wire, and weld metal produced with various welding currents.

Table II. Transformation Temperatures (K) Measured from DSC Data

	Ms _{Low}	Af _{Low}	Ms _{High}	Af _{High}
Annealed	245 (−28 °C)	272 (−1 °C)	N/A	N/A
245 A	240 (−33 °C)	271 (−2 °C)	288 (15 °C)	N/A
195 A	237 (−36 °C)	267 (−6 °C)	290 (17 °C)	292 (19 °C)
145 A	237 (−36 °C)	269 (−4 °C)	291 (18 °C)	293 (20 °C)
As received			292 (19 °C)	293 (20 °C)

D. Phase Transformations

The DSC curves for the as-received base material, heat-treated base materials, and welds produced at select weld currents are shown in Figure 10. The transformation temperatures (A_f and M_s) are summarized in Table II. The weld metal experienced multiple transformations, including a pair of high-temperature peaks and low-temperature peaks. The residual base metal on the tested specimens can account for the high-temperature peaks that had similar transformation temperatures to the as-received material. In contrast, the weld metal transformed phases at lower temperatures. The increasing welding currents showed little effect on the weld transformation temperatures.

The RMW process modified the weld metal properties so that the phase transformations occur at lower temperatures. These effects were found to be similar to annealing the base metal at 1073 K (800 °C) for 3.6 ks. This phenomenon was verified experimentally by examining the welds produced with fully annealed wires at a welding current of 195 A (Figure 11). The DSC sample underwent single-phase transformation at temperatures similar to the annealed base metal, which suggested a near homogeneous microstructure. However, the temperature range where transformation occurred was wider from the welded sample, which is likely a result of the mechanical strain imposed by the electrodes.

The intrinsic phase-transformation behavior of Nitinol is influenced strongly by thermomechanical processing. This alloy is known to exhibit broad temperature peaks when strained mechanically and narrow when annealed fully to its intrinsic state.^[12,13,21,22] Cold working can also result in higher transformation temperatures because a higher activation energy is required to overcome the internal stresses induced by random dislocations.^[13,21,22] The base metal was cold rolled and aged previously, which explained the higher transformation temperatures. During welding, the high temperatures caused a recovery of the effects of the previous thermomechanical processing, which returned the material to a near fully annealed state. A higher degree of base metal annealing occurred at a higher welding current, which resulted in more defined temperature peaks. This finding correlated well with the widening of the HAZ when the welding current was increased. Moreover, the transformation temperatures of weld metal were relatively constant at different welding currents, which suggested that the peak temperatures during welding were well above the solution-treatment temperature of 873 K (600 °C).^[23,24]

The current results showed that welding impacts the phase-transformation behavior of Nitinol significantly. Resistance heating during the RMW process anneals the original base metal, producing an HAZ with similar properties to a solid-state, solution-treated NiTi material. These local modifications in the weld zones therefore affect the functional properties of Nitinol and need to be considered in the practical application of the RMW process.

E. Effects of Pseudoelasticity and Shape-Memory Effect on RMW

Until now, the effects of pseudoelasticity and the SME properties of Nitinol on the resistance welding processes have not been discussed in the literature. However, these properties can influence the welding mechanism largely by altering the contact resistance and, consequently, the amount of resistive heating that takes place. This is true especially for crossed-wire welding in which the amount of initial cold collapse

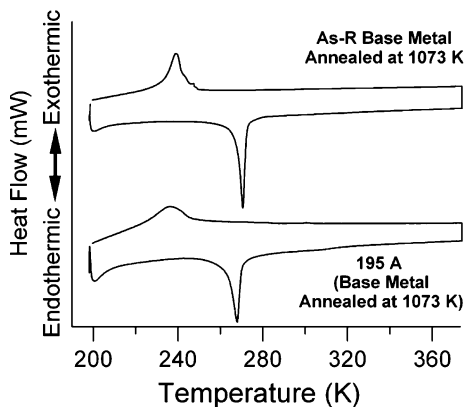


Fig. 11—DSC heating and cooling curves of annealed wire and weld made using annealed wire with 195 A current.

affects the initial contact area and, hence, resistance. Nitinol's pseudoelastic properties result in a considerably larger initial strain (*i.e.*, cold collapse) compared with 316 LVM SS crossed wires that experience the same electrode force. This result was shown experimentally by performing compression tests from 0 kg-f to the 5 kg-f electrode force on crossed Nitinol and 316 LVM SS wires, which simulated the RMW crossed-wire geometry, as illustrated in Figure 12. The maximum displacement D at the 5 kg-f electrode force plotted vs the test temperature is shown in Figure 12. At 293 K (20 °C), the initial displacement at 5 kg-f in the Nitinol wires was approximately 60 pct larger than the 316 LVM SS crossed wires. As a result, the initial contact area for Nitinol will be considerably higher, and therefore, the resistive heating at the faying interface will be lower. This observation helps explain the solid-state joining mechanism observed during the RMW of Nitinol crossed wires in both this study and that by Fukumoto *et al.*^[4] These results were interesting because it was expected that fusion welding would be possible as found during RMW of 316 LVM SS crossed wires^[6] because Nitinol and SS have similar electrical resistivity of 840 $\mu\Omega$. mm and 740 $\mu\Omega$. mm, as well as similar melting points of 1583 K (1310 °C) and 1673 K (1400 °C), respectively. Subsequently, the dynamic resistance results from this study showed that 316 SS exhibits a substantially higher initial peak resistance at the faying interface than the pseudoelastic Nitinol (Figure 13).

Compression tests performed at elevated temperatures (Figure 12) showed that pseudoelastic properties of Nitinol change with temperature. This change in properties results from increased thermodynamic stability of austenite at elevated temperatures.^[23,25] This increased stability increases the pseudoelastic plateau stress with temperature.^[23,25] At high enough temperatures Nitinol no longer exhibits pseudoelasticity and behaves much like 316 LVM SS (*i.e.*, elastic-plastic deformation) because the stress required to produce stress-induced martensite (SIM) becomes greater than the critical stress for the slip.^[23,25] Similarly, heating of the weld interface during RMW is expected to increase the local pseudoelastic plateau stress and result in an increased force exertion on the electrodes. This effect

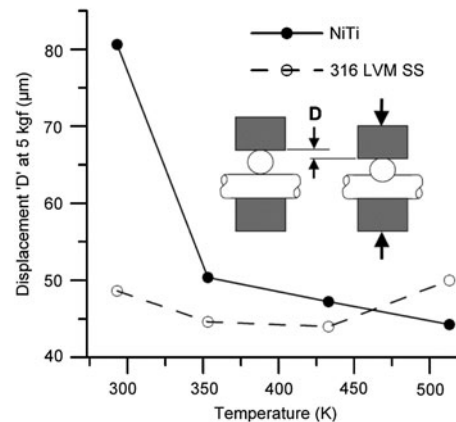


Fig. 12—Crossed-wire compression test method (a) and results (b) performed at various temperatures.

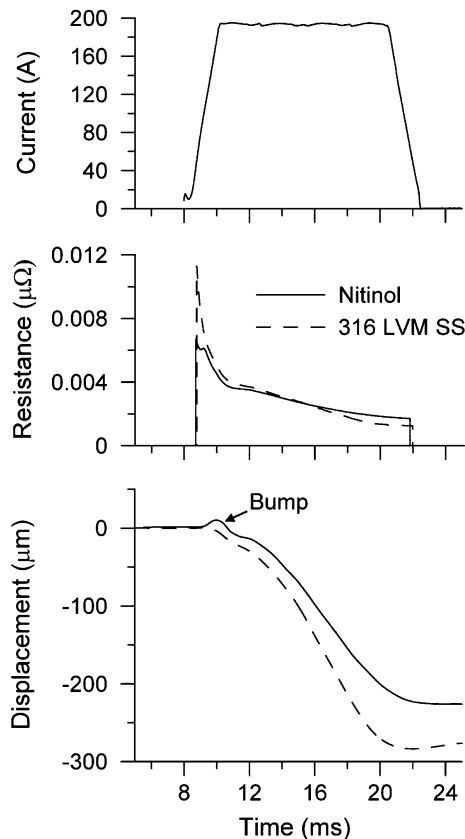


Fig. 13—Current, dynamic resistance, and displacement measured during the RMW of Nitinol and 316 LVM SS crossed wires with welding current of 200 A and electrode force of 5 kg-f.

will cause the wires to recover strain partially and revert back to their initial round shape. The DAQ measurements reveal the onset of this reversion, as observed in Figure 13 with a “bump” in the electrode displacement trend located at the onset of current. This phenomenon was not observed during the RMW of the 316 LVM SS crossed wires that do not exhibit pseudoelastic properties (Figure 13).

It is now clear that the pseudoelastic properties of Nitinol will play a role in the joining mechanism during the RMW process. The pseudoelastic property at the initial deformation affects the initial contact resistance and will also cause a change in the contact resistance at the onset of the welding current. More work, however, is required to understand more clearly the effects of pseudoelasticity on the final joint, which will be presented in a future study.

IV. CONCLUSIONS

Resistance spot welding of crossed Nitinol wires was investigated by studying the mechanical properties, microstructures, and phase transformation. The joining mechanisms were detailed with micrographs along with images of the fracture modes. The main conclusions include the following:

1. Surface cleaning was essential in RMW of Nitinol. The relative difference in the interfacial peak resistance and the electrode-to-wire interfaces compared with the resistance at the faying interface allowed heat to generate at the faying interface, minimizing electrode sticking and expulsion.
2. The joining mechanism in RMW crossed Nitinol wires was predominantly solid-state bonding consisting of six main stages, which include (1) cold collapse, (2) dynamic recrystallization, (3) interfacial melting, (4) squeeze out, (5) excessive flash, and (6) surface melting.
3. The fracture modes transitioned from interfacial failure at a low current to partial-interfacial failure at intermediate currents and, finally, to HAZ failure at high currents. A maximum joint-breaking force was attained by balancing the competing factors of increasing the interfacial bond strength and softening in the HAZ.
4. The heat generated during the RMW process locally annealed the previously strain-hardened base material leading to the modification of the transformation temperatures of the weld metal. The transformation temperatures of the weld metal were similar to those of the solution-treated material.
5. The unique pseudoelastic property of Nitinol must be considered to understand the joint formation in the RMW of Nitinol alloys more completely. Pseudoelasticity was found to cause an increase in the initial strain or cold collapse, whereas the onset of current and resistive heating causes a decrease in the strain. Both of these phenomena cause changes in the contact area, and hence, contact resistance and resistive heating.

ACKNOWLEDGMENTS

The authors acknowledge the support of National Sciences and Engineering Research Council (NSERC) of Canada. The authors also acknowledge Mr. Dennis W. Norwich of Memry Corporation for supplying the material examined in this study.

REFERENCES

1. N.B. Morgan: *Mater. Sci. Eng. A*, 2004, vol. 378, pp. 16–23.
2. Y. Zhou: *Microjoining and Nanojoining*, Woodhead Publishing, Cambridge, U.K., 2008.
3. S. Fukumoto and Y. Zhou: *Metall. Mater. Trans. A*, 2004, vol. 35A, pp. 3165–76.
4. S. Fukumoto, S. Morikawa, and A. Yamamoto: *Mater. Sci. Forum*, 2008, vols. 580–582, pp. 225–28.
5. S. Fukumoto, T. Matsuo, H. Tsubakino, and A. Yamamoto: *Mater. Trans.*, 2007, vol. 48 (4), pp. 813–20.
6. M.I. Khan, J.M. Kim, M.L. Kuntz, and Y. Zhou: *Metall. Mater. Trans. A*, 2009, vol. 40A, pp. 910–19.
7. B. Tam, M.I. Khan, and Y. Zhou: *Materials and Processing for Medical Devices*, ASM Int. Conf, Minneapolis, MN, 2009, pp. 207–09.
8. B. Tam, M.I. Khan, and Y. Zhou: *Metall. Mater. Trans. A*, 2011, vol. 42A, pp. 2166–75.

9. M. Nishikawa, H. Tanaka, M. Kohda, T. Nagaura, and K. Watanabe: *J. Phys. Colloque C4 Suppl.*, 1982, vol. 12 (C4), pp. 839–44.
10. J. Beyer, P.A. Besselink, and J.H. Lindenhovius: *Shape Memory Alloys Proceedings of the International Symposium*, 1986, pp. 492–97.
11. T. Saburi, T. Tatsumi, and S. Nenno: *J. Phys. Colloque C4 Suppl.*, 1982, vol. 12 (C4), pp. 261–66.
12. K. Kurita, H. Matsumoto, and H. Abe: *J. Alloys Compd.*, 2004, vol. 381, pp. 158–61.
13. C.P. Frick, A.M. Ortega, J. Tyber, A.El.M. Maksound, H.J. Maier, Y. Liu, and K. Gall: *Mater. Sci. Eng. A*, 2005, vol. 405, pp. 34–49.
14. W. Kiattiwongse, A. Khantachawana, and P. Santiwong: *Adv. Mater. Res.*, 2008, vols. 55–57, pp. 249–52.
15. M. Fujio, M. Masakuni, and Y. Ohura: *Euro. J. Orthodon.*, 1988, vol. 10, pp. 187–91.
16. D.W. Dickinson, J.E. Franklin, and A. Stanya: *Weld. J.*, 1980, vol. 59 (6), pp. 170–76.
17. W. Tan, Y. Zhou, H.W. Kerr, and S. Lawson: *J. Phys. D: Appl. Phys.*, 2004, vol. 37, pp. 1998–2008.
18. W. Tan, S. Lawson, and Y. Zhou: *Metall. Mater. Trans. A*, 2005, vol. 36A, pp. 1901–10.
19. Z. Zhang, J. Frenzel, K. Neuking, and G. Eggeler: *Acta Mater.*, 2005, vol. 53, pp. 3971–85.
20. S.J. Dong, G.P. Kelkar, and Y. Zhou: *IEEE Trans. Electr. Packag. Manufact.*, 2002, vol. 25 (4), pp. 355–61.
21. D.A. Miller and D.C. Lagoudas: *Mater. Sci. Eng. A*, 2001, vol. 308, pp. 161–175.
22. H. Matsumoto: *Phys. B*, 1993, vol. 190, pp. 115–120.
23. K. Otsuka and X. Ren: *Prog. Mater. Sci.*, 2005, vol. 50, pp. 511–678.
24. F. Jiang, L. Li, Y. Zheng, H. Yang, and Y. Liu: *Intermetallics*, 2008, vol. 16, pp. 394–98.
25. S. Miyazaki, K. Otsuka, and Y. Suzuki: *Scripta Metall.*, 1981, vol. 15, pp. 287–92.